Reliability and precision are optimal for non-uniform distributions of presynaptic release probability

[1,2] Jean-Marc Fellous

[1] Nadia Corral-Frías

Material and Methods – Supporting Information and Figures

Methods for Figure 1

To illustrate the consequence of recruiting high or low probability synapses on the output of a cell, we use a simple single compartment model. The neuron is contacted by 500 AMPA/NMDA synapses (see below) subdivided in two groups. The first group contains 470 synapses and is labeled 'background' the second group contains 30 synapses (6.4%, arbitrary here) and is labeled 'signal'. The background synapses receive random 5Hz Poisson presynaptic trains throughout the 500 ms simulation and each of the signal synapses receive one presynaptic input 'signal' at time 250 ms ± 10ms mimicking an input volley of 30 presynaptic spikes arriving within 20 ms of each other. All synapses have the same conductance, and are on the same compartment, so have the same elementary Excitatory Post Synaptic Potential (EPSP) if they release. The probability of these two family of synapses is uniformly fixed to either high (p=0.65) or low (0.25) values in four sets of simulations. To assess the response of the cell, the simulation is run 50 times, with the same set of presynaptic background and signal spikes and the response of the cell is plotted in a rastergram. To quantify the ability of the cell to respond to the signal, the signal to noise ratio (SNR) is computed as the number of spikes emitted between 240 ms and 275 ms (accounting for the membrane time constant of the cell, which is 10 ms, gray areas in Fig 1) divided by the total number of spikes produced.

Morphology

We used a reconstructed multi-compartmental CA1 cell from the Duke/Southampton cell archive (cell n180). This cell was chosen to represent the digitized cell population available in terms of surface area and branching structure (cells n400 and n123 were also studied with similar results, but are not discussed here for clarity). The cell membrane area was 74,686 μm^2, and contained about 600 compartments (Figure 2B). The cell surface was corrected to account for spines [1].

Cell physiology

All compartments had an axial resistance of 100 Ωcm. The compartment capacitance was increased from the standard 1 $\mu F/cm^2$ to 1.6 $\mu F/cm^2$ to account for the presence of spines [2]. In all simulations, the dendritic tree had a sigmoidal distribution of leak conductance so that distal dendritic compartments were more 'leaky' than proximal

compartments, in agreement with data collected *in vitro* in neocortex [2]. Similar experiments in hippocampus were not available. The biophysical origin of this leak is unknown, but is likely to be the result of various dendritic currents active near rest. Somatic R_m was set to 34,000 Ωcm^2 (R_{soma}) and the most distal compartment had an R_m of 5,000 Ωcm^2 (R_{end}). The half point of the sigmoid distribution was set to 400 μm and its steepness was set to 50 μm [2]. At a distance *d* from the soma, the membrane resistance was given by;

$$R_m(d) = R_{end} + \frac{R_{soma} - R_{end}}{1 - e^{\frac{400-d}{50}}} \qquad (1)$$

Active currents were located at the soma and consisted in a fast sodium current and a delayed rectifier potassium current with dynamics and conductances as in previous work [3]. A muscarinic potassium current was added to model spike frequency adaptation and adjust the cell threshold. The kinetics and conductance for this current were set as in other modeling studies [4,5]. Under these conditions, the input resistance measured at the soma by 200 pA hyperpolarizing pulses was about 60 MΩ, and the membrane time constant was about 20 ms. The resting membrane potential was kept between -70 mV and -65 mV. The voltage and current thresholds for action potential generation were about -53 mV and 500 pA respectively. These values are compatible with experimental data obtained in the hippocampal slice [6,7].

The membrane characteristics of a CA1 cell in the behaving animal are unknown. In the anesthetized preparation, CA1 resting membrane potential fluctuates around -62 mV (± 4mV) with an input resistance of about 50 MΩ, and a threshold at about -49 mV [8,9]. We further adjusted the reversal potential of the leak current to set the average membrane potential to -62 mV (the new value of this reversal potential was -55 mV). Under these conditions, the membrane potential of the CA1 cell fluctuated with a standard deviation of 3.9 mV, and its input resistance was 48 MΩ.

Model of stochastic release:

The probability of release of a single synapse was given by the equation

$$P_r(t) = 1 - e^{-F(t)/D(t)} \qquad (2)$$

where F and D are time-dependent variables representing facilitation and depression, respectively. At each excitatory synapse, when a presynaptic spike is received at time t, a random number from a uniform distribution is drawn and the probability of release, $P_r(t)$, is calculated based on the current release history S (the subset of presynaptic spike times at which the synapse has indeed released). If the random number is larger than $P_r(t)$, a postsynaptic potential is generated, and S is updated. Note that it is not necessary to update $P_r(t)$ for each synapse at every simulation time increment but only when a presynaptic spike occurs at that synapse.

$$F(t) = F_0 + \sum_{t_i < t} f(t - t_i) \text{ and } f(x) = F_{mag} e^{-x/\tau} \qquad (3)$$

F(t) is akin to an exponentially decaying accumulation of calcium with each presynaptic spike time t_i (F_0, F_{mag} and τ are constants).

$$D(t) = D_0 + \sum_{t_i < t, t_i \in S} d(t - t_i) \text{ and } d(x) = D_{mag} e^{-x/\tau'} \qquad (4)$$

where S is the dynamically updated set of spike times that yielded release (D_0, D_{mag}, τ' are constants).

The initial probability of release is therefore given by:

$$p_0 = 1 - e^{-F0/D0} \qquad (5)$$

Because F(t) and D(t) have arbitrary units, we choose D_0=1. Therefore p_0 is determined by F_0. We note that biophysically, p_0 depends on the size of the releasable vesicle pool, and the probability of release of a single vesicle. We do not expand p_0 here in terms of these factors. The parameters, F_0, F_{mag} and D_{mag} are therefore in units of D_0.

Depression:

Time constant of depression:

Depression is the result of vesicle depletion and a reduction in synaptic vesicle release probability. We aggregate these two phenomena here and show that this simplification is not detrimental to the match of the model to data. Depression is expressed as an instantaneous decrease in release probability (D_{mag}) only if the synapse has released. This condition constitutes a fundamental difference with all 'average' models that compute and use average probability, because, in our case, depression occurs only in response to a subset of the presynaptic spikes (unlike facilitation, which occurs at every presynaptic spikes). After release, the decrease in probability slowly recovers with time constant τ'. This time constant is typically slow (2-20s time scales) [10]. Because we limit our simulations to times scales compatible with that of a rat traversing a place field (2-3 sec, at normal speeds), we set this value to 2.5 seconds. Larger values did not significantly change the results presented here (tested for 5 and 10 sec, not shown).

Magnitude of depression

In order to adjust the magnitude of depression D_{mag}, we use 100 trials of 24 presynaptic pulse trains at 10 Hz, as in experiments [10]. In single CA1 synapses, synaptic depression in response to this stimulation protocol has time constants varying from 220 ms to 490 ms, depending on the amount of facilitation present, and is in the 300 ms to 400 ms range in synapses with no facilitation [10]. Because these experiments were conducted in high [Ca]/[Mg] ratios, the actual depression time constant at single synapse is expected to be somewhat larger. Unfortunately no quantitative (average) data were provided in this work. Using equations 2-5, setting F_{mag} to 0 (no facilitation), and using a distribution of F_0 yielding $N(p_0)$ as in Fig 2A, D_{mag} is completely constrained by the experimental data from synapses that do not show facilitation. Figure S1A shows the results of the simulations.

For synapses with high initial release probability, D_{mag} was found to be about 1 (in units of D_0) and the decay time constant of depression was 510 ms, compatible with experimental data (Figure S1A). The use of lower initial probability synapses increased this time constant (e.g. if p_0=0.5 the depression decay time constant was 900 ms). With lower probabilities (<0.4), the variability of responses significantly decreased the quality of the exponential fit, and the estimation of the time constant became unreliable.

Validation: In imaging experiments, paired pulse stimulation of cultured single synapses in 3mM-Ca/1mM-Mg showed that facilitation was abolished, and only synaptic depression remained [11]. Depression was found to have two components: a decrease in quantal size, and a decrease in probability of release. While a decrease in quantal size was not observed in the acute experiments of [10], our model, as tuned, should capture the decrease in probability measured by those imaging experiments. We ran simulations of synapses with various initial release probability, with facilitation blocked, stimulated by two pulses 50 ms apart, as in the experiments [11]. Figure S1B shows that, without further parameter tuning, the model exhibited a linear relationship between the probability of release during the first pulse (p_0, initial probability of release), and probability of release during the second pulse. The slope of the linear fit was 0.75, each point representing the average of 200 paired pulses. Three synapses from the imaging experiments for which these probabilities were given are plotted (open circles) and fall well within the predictions generated by the model.

Facilitation:

Time constant of facilitation:

At most CA3-CA1 synapses, facilitation has two temporal components with time constants of about 40 ms and 400 ms. As noted in other work, these two components are often well fitted by a single exponential decay function [12]. We choose here τ=120 ms, compatible with recordings made in hippocampus ([13], fitted from their Figure 1). This time constant is comparable to others obtained *in vitro* in cortex (94 -242 ms [14]), and used in other models (cortex, medium facilitation component: 190 ms [15]).

Magnitude of facilitation

Experimental evidence suggests that the magnitude of facilitation depends on the initial probability of release [16]. Our mathematical expressions (eqs 2-5) are amenable to a formal analytical derivation of this dependence.

Paired-pulse facilitation: Analytical derivation

For both a 40 ms inter-pulse interval [10] and a 50 ms interval [17], the probability of release at the time of the second pulse p_2 is well described by

$$p_2 = 1-(1-p_0)^{\frac{1}{\sqrt{p_0}}} \qquad (6)$$

In these experiments, p_2 resulted presumably from an interaction between facilitation and depression. Using our formulation (Equation (2-5)), we have therefore:

$p_2 = (1-p_0)(1-e^{-F/D_0}) + p_0(1-e^{-F/D_1})$ with

$F = F_0 + F_{mag}e^{-\frac{\Delta t}{\tau}}$ and $D_1 = D_0 + D_{mag}e^{-\frac{\Delta t}{\tau'}}$ if the synapse has released on the first pulse, and $D_1=D_0$ otherwise.

With Δt=50 ms, τ=120 ms, τ'=2500 ms, D_0=1, D_{mag}=1 and F_0=-log(1-p_0). F_{mag} is therefore a completely constrained function of p_0.Using the equations above we therefore have:

$$(1-p_0)^{\frac{1}{\sqrt{p_0}}} = (1-p_0)e^{-F/D_0} + p_0 e^{-F/D_1} \qquad (7)$$

Under the assumption that p_0 is small, the synapse is unlikely to have released on the first pulse, if p_0 is large (close to 1) the synapse is likely to have released on the 1st pulse, the equation can be simplified to:

$$F_{mag} = -A\frac{\log(1-p_0)}{\sqrt{p_0}} + B \qquad (8)$$

where A and B are constants.

The values of the constants A and B were determined from simulations. For p_0<0.5, A=-1.03, B=0.00546, for p_0>0.5 A=-1.52 and B=-0.38.

Minimal stimulation [10,18] and *in vitro* imaging experiments [17] demonstrated that the amount of paired pulse facilitation was inversely related to the initial release probability of a synapse. In our simulations, the ratio between the probability of release at the second pulse to the initial probability of release P_0 was about 2 for low reliability synapses (P_0=0.1) and 1 for reliable synapses (P_0=1).

Validation: Fixing all parameters as above, we use the analytical expression of the probability of release on two consecutive pulses and hence of paired pulse facilitation (PPF). Figure S1C shows the average ratio over 20 PPF trials for 5000 synaptic locations (error bars)(green, Equation 8). For comparison, data obtained *in vitro* are plotted on the same graph (circles) [10]. The behavior of the model is well within the variability of observed experimental data. Note that the standard errors of the simulations generally decrease as initial release probability increases, qualitatively matching the experimental data. Note also that the data were obtained from different cells, in different slices, and that therefore variability is expected to be somewhat higher than that of the model. Equation (8) is therefore a good fit to the data, and F_{mag} is completely and uniquely determined by p_0.

In sum, each individual synapse had five parameters: The unitary conductance, the initial amount of facilitation and depression (F_0 and D_0 respectively), the amount of facilitation produced by a single presynaptic action potential (F_{mag}), and the amount of depression resulting from a single release (D_{mag}).

Synaptic conductances.

AMPA: Experimental work *in vitro* shows AMPA EPSC amplitude (measured by voltage clamp at -60mV at the soma, inhibitory neurotransmission blocked) was about 14 pA when putative single synapses were stimulated [10,13]. This value is compatible with recordings from isolated synaptic boutton stimulation [11] and other hippocampal minimal stimulation data (AMPA EPSCs: 15.8 ± 7.6 pA at -80 mV [19]). EPSC amplitude is not correlated with the initial release probability of the synapse [19]. In these experiments, slices are stimulated in the stratum radiatum, activating Schaffer collaterals that make contacts on the part of the CA1 dendritic arbor that is in that stratum (main trunk and secondary branches, Figure 2B, dashed lines).

NMDA: The contribution of NMDA currents to EPSCs is highly variable from synapses to synapse. AMPA and NMDA EPSCs probabilities were experimentally found to be identical at the same synapses [19]. A proper quantification of the amount of NMDA current is complicated by the possible presence of silent synapses. We use here a NMDA/AMPA ratio of 1 to match the experimental data obtained in hippocampus CA1 of the adult rat [20].

In order to adjust the synaptic conductances in our model, we computed the average somatic EPSC resulting from the random placements of 500 single synapses in the stratum radiatum, discharging one at a time. In our passive dendritic tree models, the average of the EPSC amplitudes at -60 mV was typically equal to their standard deviation and hence followed a Poisson distribution (not shown). We found that a unitary synaptic conductance of 2.9 nS yielded an average EPSC size at the soma of 14.4 pA (± 14.5). Note that this value did not depend on the release probability of the synapse (i.e. the synapse potency is independent of initial release probability [10]). The average size of the EPSCs measured in the same compartment as the synapse was 56.0 pA (± 14.4) again compatible with data obtained from dendritic recordings [21]. The same average somatic currents could be obtained with a non-uniform distribution of AMPA channels that had a perisomatic conductance of 1.1 nS, increasing linearly (2.2 nS, 200 μm from the soma).

Validation: To further verify our tuning, we fixed all parameters, repeated the simulations above in current clamp mode (Vm at rest was set to -64 mV), and measured unitary EPSPs at the soma. The mean EPSP amplitude was 361 μV (± 329), compatible with data obtained in different experiments from connected CA3-CA1 pairs in the slice (400μV, for minimal EPSPs) [22].

At this point, all parameter values of the single synapse model have been constrained to experimental data. The only free variable remaining is the total number of synapses stimulated.

Postsynaptic synaptic currents

The dynamics of the postsynaptic AMPA current was obtained upon release using a two state kinetic scheme, NMDA channels were similarly modeled with 5 states, including desensitization and resensitization [23]. The size of the unitary EPSC measured at the soma was assumed to be constant and independent of the presynaptic stimulation patterns, compatible with single-synapse data obtained in hippocampus [24]. Short term synaptic

dynamics were found to be largely independent of the level of activation or desensitization of AMPA receptors in cortex and hippocampus [10,14,18]. Therefore, synaptic conductance and short term dynamics could be adjusted independently. There is some evidence using excised patches that AMPA synaptic conductance may increase by a factor of two to four from the perisomatic area (50 μm) to more distal locations (300 μm) [21,25,26]. Most of the data come from recordings from the main trunk, and little is known of the scaling in other dendritic areas. For comparisons, simulations were performed with synaptic conductances linearly scaled by a factor two at 200 μm from the soma. As will be indicated below, such conductance scaling had no significant impact on the conclusions presented here.

Postsynaptic macroscopic currents

To simulate the response to extracellular stimulations of the Schaffer collaterals, we distribute N synapses randomly within the stratum radiatum. This assumption is justified by the finding that when a single site is stimulated with the same stimulation pattern on two (presumably) different pathways, the responses at that site are similar [24]. This suggests that even though the synapses stimulated were different, the response remained on average the same. Hence the synaptic location was as 'random' in one pathway as it was on the other. The same stimulation pattern in a different slice (hence different CA1 neuron morphologies) would result in markedly different responses. This was successfully modeled here by substituting different cell morphologies (data not shown). The synaptic density was presumed to be constant throughout the dendritic tree, and was set to 32 synapses per 100 μm^2 of dendritic area, compatible with EM data [27]. When stimulated to mimic extracellular stimulation, all N synapses received a presynaptic spike simultaneously. This assumption is justified by the finding that the standard deviation of single synapse EPSCs latencies obtained with minimal stimulations was well below 1 ms [19].

Extracellular stimulation yields a compound EPSC at the soma, which is the result of probabilistic release at N synapses. The number of synapses activated by such stimulation is experimentally unknown. Having constrained the distribution of initial release probabilities, and the unitary conductance, we now vary the number of synapses to match the range of EPSC amplitudes measured experimentally with extracellular recordings (100-500 pA). Figure S2A shows that the average EPSC measured at the soma is a linear function of the number of synapses (each point represents the mean and standard deviation of 100 trials with a fixed number of CA3 synapses distributed randomly on the dendritic tree). The inset shows the shape of an EPSC obtained with 100 synapses. The slope of the linear fit to the data is about 2.5 (solid line). Therefore, our model predicts that an extracellular Schaffer collateral stimulation yielding 100-500 pA EPSCs at the soma is the result of the recruitment of only 25-180 synapses with release probabilities and conductances described as above. Using scaled EPSCs, the slope of the fit is 2.2 (Figure S2A, dashed line) and 25-210 synapses yield somatic amplitudes in the 100-500 pA range, not significantly different from unscaled AMPA conductances. For comparison, the figure also shows the linear fit if the distribution of initial probability is Gaussian (mean=0.28, std=0.1), and therefore does not include the high probability synapses (Figure 2C, dash-dot line). The slope of the linear fit depends on the average initial probability of the synapses and is steeper

for Gaussian distributions with higher average probability (Figure S2A: $<p_0>$= 0.5, slope = 4, $<p_0>$= 0.1, slope=1.4, data points not shown for clarity).

Validation: The variability of EPSC sizes can be measured by the coefficient of variation of EPSC amplitudes. In our simulations, it was a decreasing function of the number of synapses and could be fitted by an exponential function with a 39 synapse decay constant (Fig S2B). Experimental data obtained in slices with EPSCs measuring 204 ± 53 pA revealed EPSC variability of about 15.8% ± 3.4 [6]. According to Figure S2A, about 100 synapses (unscaled conductance) are likely to have been stimulated in these experiments to yield an EPSC average of this amplitude. The corresponding variability in our model was about 19%, compatible with the experimental findings (Figure S2B, upper arrow). This value is not significantly different from that obtained with scaled AMPA conductances (18%, not shown). Note that the model variability asymptotically approaches about 14%, a value even closer to that of the experimental data (15.8% ± 3.4). For comparison, we plot the CV of EPSC amplitudes when the initial probability distribution is Gaussian centered at the same mean as $N(p_0)$ (mean=0.28, standard deviation=0.1, Figure S2B dashed line). This distribution does not include the high probability synapses that form the tail of the experimentally derived distribution (Figure 1B). For this distribution, the CV is significantly higher and would enter the experimental range of 15.8% ± 3.4 at about 300 synapses. Figure S2A shows however that such a number of synapses would yield a somatic EPSC of about 800 pA, which is incompatible with what was obtained experimentally (204 ± 53 pA). Our model therefore suggests that a naïve, Gaussian-like distribution of initial probability cannot satisfy both the variability and the size of the somatic EPSC observed experimentally.

To complement the study of EPSC variability, and further validate our model, the variability of EPSPs measured at the soma was assessed by stimulating N synapses 50 times, and by computing the coefficient of variation of EPSP amplitudes, while the cell was slightly hyperpolarized to avoid spiking (-250 pA, as in experiments). The CV was a decreasing function of N that could be well fitted by an exponential function with a decay constant of 46 synapses. To compare with data, using the assumption above that about 100 synapses were stimulated, our simulations show that the EPSP variability is about 13%, (S2B, lower arrow) again, compatible with experimental data (13.7% ± 3%) [6]. This value is not significantly different from that obtained with scaled AMPA conductances (16%, not shown). Again, the model asymptotically converges close to the value observed experimentally.

Taken together, these modeling results suggest that most extracellular stimulations of the Schaffer collaterals *in vitro* recruit a low number of synapses in the range of 100 or less, and that a skewed distribution of initial release probability (Figure 2A) is required to account for both the variability and the size of the postsynaptic currents observed experimentally *in vitro*.

Input spike trains

The inputs spike trains to our model CA1 cell were taken from a population of 37 CA3 pyramidal cells recorded simultaneously in four 10 minutes sessions, as the animal was exploring a rectangular box [28]. For each cell, place

fields were characterized using video tracking data (single place fields). Each traversal of each place field of each cell was isolated, and the corresponding spike trains were collected. Figure S3A shows 300 of the 992 CA3 spike trains thus collected. Spike trains contained all the classical characteristics of CA3 place cells, including bursts and theta modulation. For technical reasons, it is not possible to record from more than about 100 cells simultaneously. To simulate N CA3 inputs to a CA1 cell (N up to 900 here), we randomly picked from the 992 spike trains obtained by the procedure above, and made the assumption that the variability observed in randomly picking N spike trains out of 992 place field traversals of 37 CA3 cells was similar to that of N different CA3 cells recorded simultaneously as the animal traverses a single region of space only once. The inset of Figure S3A shows the distribution of CA3 mean firing rates during place field traversal (4.7 ± 4.3 Hz, computed in a 4 second window centered on the crossing of the center of the field as displayed in the rastergram). In the same manner, 1878 spike trains were collected in the same apparatus, from 26 simultaneously recorded CA1 place cells exhibiting a well defined and unique place field. These spike trains are used to assess the response of the model CA1 cell.

At least two presynaptic features can affect the firing rate of the CA1 cell in a particular environment; the number of CA1 synapses recruited during the place field traversal (number of CA3 place fields overlapping with the CA1 place field), and the mean firing rate of the presynaptic CA3 cells. A change in the population of presynaptic CA3 synapses recruited mimics the CA3 component of global remapping. A change in the firing rate of a fixed set of CA3 synapses mimics rate remapping [29].

Choosing a realistic number of input CA3 synapses

Figure S3B shows the in-field firing rate of the simulated CA1 cell for different numbers of presynaptic CA3 cells (assuming one synapse per CA3 cell). In the range of 200 to 800 synapses, the firing rate increases quasi-linearly with the number of CA3 synapses recruited. In these simulations, different sets of synapses are randomly selected for each X-axis value. Experimental CA1 cells in-field firing rates measured simultaneously with CA3 were 3.6 Hz ± 2.7Hz (2B horizontal lines). This modeling result suggests therefore that, if CA3 alone was involved in discharging CA1, the number of CA3 place cells involved in the traversal of one CA1 place field would be about 500 ± 200. Note that since CA1 also receives inputs from the entorhinal cortex, the actual number of CA3 inputs involved in discharging a given CA1 cell is likely to be smaller. A statistical analysis of the simulation results shows that a differential of 75-125 CA3 synapses is required to change the CA1 firing rate significantly (paired t-tests between consecutive points in the graph, $p<0.05$). This suggests that global remapping (change in CA3 afferent synapse population) will not affect a CA1 cell unless at least 75-125 CA3 cells remap spatially. While the exact number of synapses yielding significance depends on the number of samples and other parameters of our simulations, this result suggests that global remapping will occur only after a sufficient number of individual cells have remapped. According to this model, global remapping has a 'threshold' (here of about 75-125 cells) below which the mapping should be spatially robust.

Figure S3C shows the mean CA1 firing rate (40 trials per points) as a function of the mean firing rate of the CA3 inputs (500 fixed synapses, randomly distributed on the dendritic arbor in the stratum radiatum). The slope was 0.8 Hz/Hz. A paired t-test analysis on consecutive points indicated that a differential of about 1.3Hz in CA3 firing

rates was necessary for the CA1 cell to generate significantly different firing rates. The arrow points to the nominal CA3 mean firing rate obtained from 500 of the 992 spike trains in panel A. The inset shows a sample voltage trace from the simulated CA1 cell responding to one trial with 500 synapses. This result suggests that a rate remapping in CA3 will not be detected by CA1 unless the average firing rate in CA3 changes by more than 1.3 Hz.

These results justify our choice of 500 CA3 input synapses.

Reliability and Precision

To quantify their occurrence we use the 'direct method' for the computation of reliability and precision [30]. Briefly, a histogram is constructed from the 40-trial rastergram (15 ms bins) and smoothed (Gaussian kernel of 6 ms). A threshold is computed as 4 standard deviations away from the mean of the smoothed histogram. All threshold crossings are termed 'events' and correspond to alignments in the 40-trial rastergram. The width of each event is computed as the width of the smoothed histogram peaks at mid-height. All spike times falling within the width of any event are counted as reliable spikes. The reliability R if the fraction of all the spikes generated by CA1 that fall within a reliable event across the 40 trials ($0 \leq R \leq 1$).

The standard deviation σ_e of the spike times falling in each event is computed. This value gives an indication of the jitter with which reliable spikes are produced, for each specific event. The average jitter σ is computed across all events in the rastergram. We define the precision of the response as $P=1/2\sigma$. P is expressed in Hertz and can be interpreted as the maximal frequency at which a cell which generate spikes with a jitter of standard deviation σ when driven so that it generates only one spike in at least 50% of all the cycles (i.e. above chance). P/2 is the maximal driving frequency that would generate exactly 1 spike per cycle (the period of this frequency is 4σ, approximately the width at the base of a Gaussian distribution of standard deviation σ). Both R and P are specific to the particular CA3 presynaptic spike pattern used to obtain the 40-trial rastergram.

References cited

1. Major G, Larkman AU, Jonas P, Sakmann B, Jack JJ (1994) Detailed passive cable models of whole-cell recorded CA3 pyramidal neurons in rat hippocampal slices. J Neurosci 14: 4613-4638.
2. Stuart G, Spruston N (1998) Determinants of voltage attenuation in neocortical pyramidal neuron dendrites. J Neurosci 18: 3501-3510.
3. Traub RD, Jefferys JG, Miles R, Whittington MA, Toth K (1994) A branching dendritic model of a rodent CA3 pyramidal neurone. J Physiol 481: 79-95.
4. Yamada W, Koch C, Adams PR (1989) Multiple Channels and Calcium Dynamics. In: Koch C, Segev I, editors. Methods in Neuronal Modeling: From synapses to Networks. Cambridge, Massachusets: M.I.T. Press. pp. 97-133.
5. Gutfreund Y, Yarom Y, Segev I (1995) Subthreshold oscillations and resonant frequency in guinea-pig cortical neurons: physiology and modelling. J Physiol (Lond) 483: 621-640.
6. Otmakhov N, Shirke AM, Malinow R (1993) Measuring the impact of probabilistic transmission on neuronal output. Neuron 10: 1101-1111.
7. Altemus KL, Lavenex P, Ishizuka N, Amaral DG (2005) Morphological characteristics and electrophysiological properties of CA1 pyramidal neurons in macaque monkeys. Neuroscience 136: 741-756.

8. Henze DA, Buzsaki G (2001) Action potential threshold of hippocampal pyramidal cells in vivo is increased by recent spiking activity. Neuroscience 105: 121-130.
9. Isomura Y, Sirota A, Ozen S, Montgomery S, Mizuseki K, et al. (2006) Integration and segregation of activity in entorhinal-hippocampal subregions by neocortical slow oscillations. Neuron 52: 871-882.
10. Dobrunz LE, Stevens CF (1997) Heterogeneity of release probability, facilitation, and depletion at central synapses. Neuron 18: 995-1008.
11. Chen G, Harata NC, Tsien RW (2004) Paired-pulse depression of unitary quantal amplitude at single hippocampal synapses. Proc Natl Acad Sci U S A 101: 1063-1068.
12. Zucker RS, Regehr WG (2002) Short-term synaptic plasticity. Annu Rev Physiol 64: 355-405.
13. Dobrunz LE, Huang EP, Stevens CF (1997) Very short-term plasticity in hippocampal synapses. Proc Natl Acad Sci U S A 94: 14843-14847.
14. Varela JA, Sen K, Gibson J, Fost J, Abbott LF, et al. (1997) A quantitative description of short-term plasticity at excitatory synapses in layer 2/3 of rat primary visual cortex. J Neurosci 17: 7926-7940.
15. Matveev V, Wang XJ (2000) Differential short-term synaptic plasticity and transmission of complex spike trains: to depress or to facilitate? Cereb Cortex 10: 1143-1153.
16. Thomson AM (2000) Facilitation, augmentation and potentiation at central synapses. Trends Neurosci 23: 305-312.
17. Murthy VN, Sejnowski TJ, Stevens CF (1997) Heterogeneous release properties of visualized individual hippocampal synapses. Neuron 18: 599-612.
18. Hanse E, Gustafsson B (2001) Factors explaining heterogeneity in short-term synaptic dynamics of hippocampal glutamatergic synapses in the neonatal rat. J Physiol 537: 141-149.
19. Hanse E, Gustafsson B (2001) Quantal variability at glutamatergic synapses in area CA1 of the rat neonatal hippocampus. J Physiol 531: 467-480.
20. Hestrin S, Nicoll RA, Perkel DJ, Sah P (1990) Analysis of excitatory synaptic action in pyramidal cells using whole-cell recording from rat hippocampal slices. J Physiol 422: 203-225.
21. Smith MA, Ellis-Davies GC, Magee JC (2003) Mechanism of the distance-dependent scaling of Schaffer collateral synapses in rat CA1 pyramidal neurons. J Physiol 548: 245-258.
22. Sayer RJ, Friedlander MJ, Redman SJ (1990) The time course and amplitude of EPSPs evoked at synapses between pairs of CA3/CA1 neurons in the hippocampal slice. J Neurosci 10: 826-836.
23. Destexhe A, Mainen ZF, Sejnowski TJ (1996) Kinetic models of synaptic transmission. In: Koch C, Segev I, editors. Methods in neuronal modeling. Cambridge: M.I.T. Press.
24. Dobrunz LE, Stevens CF (1999) Response of hippocampal synapses to natural stimulation patterns. Neuron 22: 157-166.
25. Andrasfalvy BK, Magee JC (2001) Distance-dependent increase in AMPA receptor number in the dendrites of adult hippocampal CA1 pyramidal neurons. J Neurosci 21: 9151-9159.
26. Magee JC, Cook EP (2000) Somatic EPSP amplitude is independent of synapse location in hippocampal pyramidal neurons. Nat Neurosci 3: 895-903.
27. Harris KM, Jensen FE, Tsao B (1992) Three-dimensional structure of dendritic spines and synapses in rat hippocampus (CA1) at postnatal day 15 and adult ages: implications for the maturation of synaptic physiology and long-term potentiation. J Neurosci 12: 2685-2705.
28. Leutgeb S, Leutgeb JK, Treves A, Moser MB, Moser EI (2004) Distinct ensemble codes in hippocampal areas CA3 and CA1. Science 305: 1295-1298.
29. Colgin LL, Moser EI, Moser MB (2008) Understanding memory through hippocampal remapping. Trends Neurosci.
30. Tiesinga P, Fellous JM, Sejnowski TJ (2008) Regulation of spike timing in visual cortical circuits. Nat Rev Neurosci 9: 97-107.

Supplemental Figures

Figure S1: Tuning and validation of synaptic parameters. A: Somatic EPSC amplitude in response to a train of 24 pulses at 10Hz. The exponential fit (red curve) gives a time constant of 510 ms. B: Validation of the synaptic

parameters of depression: After the tuning achieved in A, all other parameters fixed, the model was run on a new experimental paradigm: Paired pulse (50 ms ISI) protocol for synapses with various initial probability of release. Red circle are from actual data (Chen et al. 2004). C: Validation of the synaptic parameters for facilitation. Pair-pulse facilitation ratio (50 ms ISI) is plotted as a function of initial release probability. Points with error bars: simulation data showing the average and standard deviation of the PPF ratio computed at 5000 locations in the dendritic tree, each averaged across 20 trials. Circles: Data from Dobrunz et al. (1997). Continuous curve: Continuous fit (eq 6) from Dobrunz et al. (1997).

Figure S2: Tuning and validation of postsynaptic currents. A: Somatic EPSC as a function of the number of CA3 synapses stimulated. Circles and error bars: simulation data (100 trials). Dashed line indicate EPSC size typically recorded experimentally (100-500 pA) suggesting a recruitment of 25-180 synapses. Solid line is the linear fit. Dash-dot line is the linear fit for a Gaussian distribution of initial release probability centered at 0.28 ± 0.1, data points not shown for clarity). Dashed line is the linear fit for scaled AMPA conductances. Two other solid lines are fits for Gaussian distributions of initial probabilities centered at 0.5 and 0.1 (data points not shown for clarity). B: Validation of the tuning in A. Coefficient of variation of EPSP (positive values) and EPSC (negative values) plotted on the same graph, as a function of the number of synapses stimulated. Arrows point to values measured experimentally by Otmakhov et al. (1993): 15.8% for EPSCs and 13.7% for EPSPs. Continuous line is an exponential fit to the simulation data. Dashed line is the exponential fit when the initial probability of release is distributed as a Gaussian centered at 0.28 (with no high probability tail, data points not shown for clarity).

Figure S3: Firing during place field traversal. A: rastergram showing 300 of the 992 spike trains obtained from 37 simultaneously recorded CA3 single-place-field cells (Leutgeb et al. 2004). Spike trains were aligned at the center of their respective place fields. The inset shows the distribution of CA3 firing rates. B: Mean firing rate of the CA1 cell as a function of the number of presynaptic CA3 inputs. All CA3 synapses were stimulated with inputs randomly drawn from 2A. C: Mean firing rate of the CA1 cell in response to variations in the mean CA3 firing rate (500 synapses). The arrow point to the mean firing rate as measured in the data (random sampling from 2A). The four other points were obtained by re-sampling 500 spike trains from 2A so that the CA3 mean firing rate varied between 1 and 8 Hz. Inset: sample voltage trace of the CA1 cell stimulated by 500 synapses (arrow). Scale bar is 10 mV, 500 ms.

Supplemental figures

Figure Supp.1

A

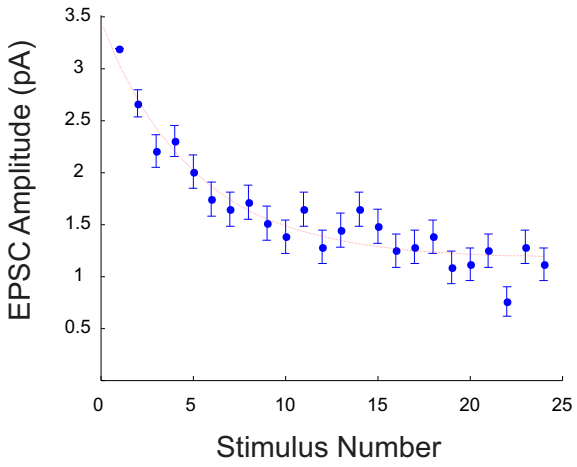

B

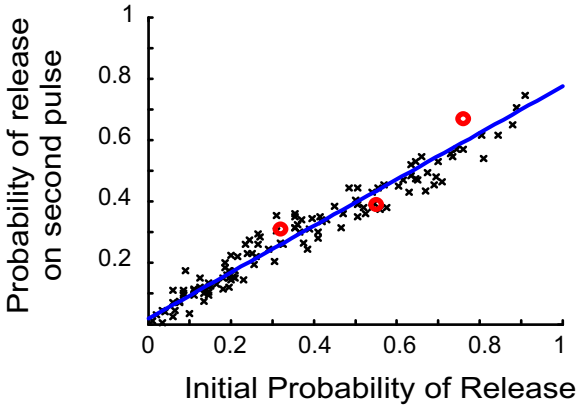

C

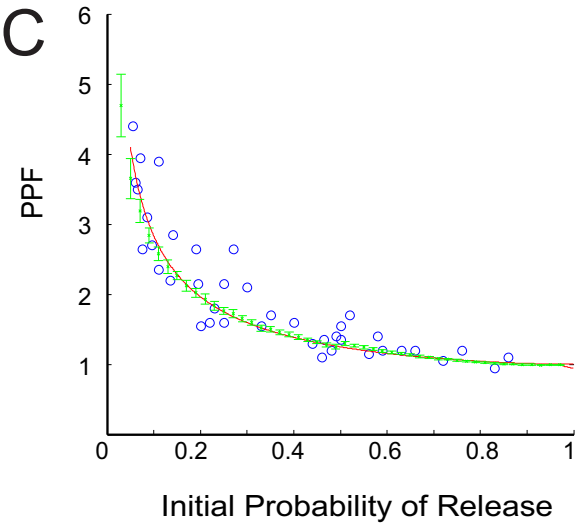

Supplemental figures

Figure Supp.2

A

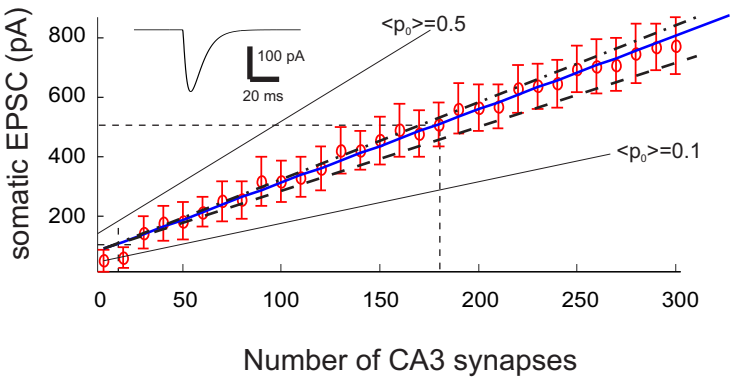

B

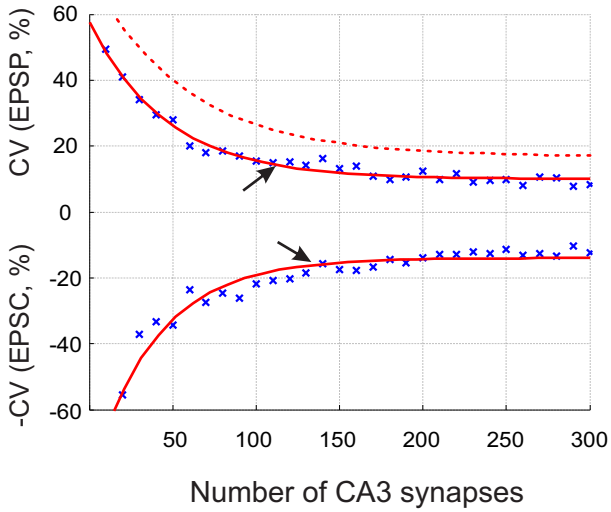

Supplemental figures
Figure Supp.3